Light-Triggered, Enhancement-Mode AlInN/GaN HEMTs With Sub-Microsecond Switching Times

Elia Palmese, *Member, IEEE*, Haotian Xue, Daniel J. Rogers, *Member, IEEE*, and Jonathan J. Wierer Jr., *Senior Member, IEEE*

***Abstract*— Light-triggered, AlInN/GaN high-electron-mobility transistors (HEMTs) are presented. Selective thermal oxidation of the AlInN barrier between the source and drain depletes the AlInN/GaN 2-dimensional electron gas, enabling enhancement mode operation and light-triggering capability. A commercially available 375 nm laser diode is focused on the bare (no metal) oxidized gate, and despite being below bandgap, it triggers the HEMT into the on-state. The HEMTs have a peak saturation current of ~60 mA/mm, switch at 100 kHz, exhibit sub-microsecond switching times which are faster than other GaN-based switching devices, and are limited by the laser power supply.**

***Index Terms*— Enhancement-mode HEMTs, light triggered, AlInN/GaN, AlInN oxidation.**

I. Introduction

WIDE bandgap (WBG) semiconductors such as SiC and GaN have facilitated advancements in power devices. They are preferred over silicon because of their higher switching speeds, lower conduction loss, higher operating temperatures, and higher figure-of-merit [1], [2], [3]. Rapid switching offers a huge opportunity to reduce circuit losses, relax thermal management, and improve converter power density. However, faster switching can lead to oscillations, causing large voltage and current overshoots, electromagnetic interference (EMI), and device damage. Reduction in EMI is the greatest limiter in higher switching frequencies, and one method to reduce it is to employ optically driven (light-triggered) power devices [4], [5].

Light-triggering in high-voltage switching-capable devices has been demonstrated in Si- and SiC-based photoconductive semiconductor switches (PCSSs) and thyristors [6], [7], [8], [9]. For GaN, light-triggering or optical excitation is an emerging area, with demonstrations of PCSSs [10], [11], photodiodes (PDs), and phototransistors (PTs) using high-electron-mobility transistor (HEMT) structures [12], [13]. HEMTs are a potential light-triggered power device but with two major limitations. First, the 2-dimensional electron gas (2DEG) formed at the AlGaN/GaN or AlInN/GaN heterointerface causes high dark currents [14], [15], [16]. Cascode configurations, recessed gates, and p-GaN gates are methods to mitigate high dark currents [17], [18], [19], [20], [21]. Secondly, these demonstrations exhibit slow switching speeds with fall times in the 100's of milliseconds or greater due to persistent photoconductivity (PPC) [22]. Possible causes for PPC in GaN devices include deep-level defects, vacancies, and metastable defects from dopants [23], [24], [25].

This letter addresses the aforementioned limitations to create AlInN/GaN light-triggered HEMTs (LT-HEMTs). The LT-HEMTs have a gate consisting of selectively oxidizing approximately half of the AlInN barrier thickness [26] in a region between the source and drain contacts. The AlInN/GaN interface below the oxidized AlInN depletes the 2DEG, creating an enhancement-mode (E-mode) AlInN/GaN HEMT [27], [28]. Under the illumination with a 375 nm laser, carriers are generated under the oxidized gate, which increases source-to-drain conductivity and turns on the HEMT. The LT-HEMTs switch at 100 kHz and exhibit sub-microsecond response times, which are limited by the laser power supply.

II. Experimental Methods

The LT-HEMT epitaxial structure is grown on silicon substrates. It consists of a 700 nm unintentionally doped (UID) GaN layer, a ~1 nm thick AlN layer, and a 10 nm thick UID doped $Al_xIn_{1-x}N$ barrier layer with x=0.82, and has a sheet resistivity of 280 Ω/square. Device processing begins by forming a mesa etched 400 nm deep. Then, a 43 nm thick SiN_x layer is deposited and patterned to open 2 μm and 5 μm long regions for selective oxidation. The sample is then loaded into a horizontal quartz tube furnace and subjected to dry thermal oxidation [27], [29] at 850 °C for 30 minutes with ~2800 sccm of O_2. Finally, the SiN_x mask is removed, and Ti/Al/Ni/Au ohmic source and drain metal contacts are formed. The surface of the devices is not passivated.

Fig. 1(a) shows a top-view microscope image of the LT-HEMT with a 2 μm long oxidized gate. The tested devices with two different gate lengths (2 μm and 5 μm) are 190 μm wide but have different lengths between the source and gate (L_{SG}) and gate and drain (L_{GD}). Table I summarizes the device dimensions and the 2DEG resistance (R_{2DEG}).

For DC testing, the current versus voltage characteristics (I_D vs V_{DS}) are measured with a semiconductor parameter analyzer. A commercial 375 nm laser (KVANT) illuminates

Manuscript received 24 July 2024; accepted 5 August 2024. Date of publication 7 August 2024; date of current version 27 September 2024. This work was supported by the U.S. National Science Foundation under Award 2212639. The review of this letter was arranged by Editor R.-H. Horng. *(Corresponding authors: Elia Palmese; Jonathan J. Wierer Jr.)*

The authors are with the Department of Electrical and Computer Engineering, North Carolina State University, Raleigh, NC 27695 USA (e-mail: ejpalmes@ncsu.edu; jjwierer@ncsu.edu).

Color versions of one or more figures in this letter are available at https://doi.org/10.1109/LED.2024.3440177.

Digital Object Identifier 10.1109/LED.2024.3440177

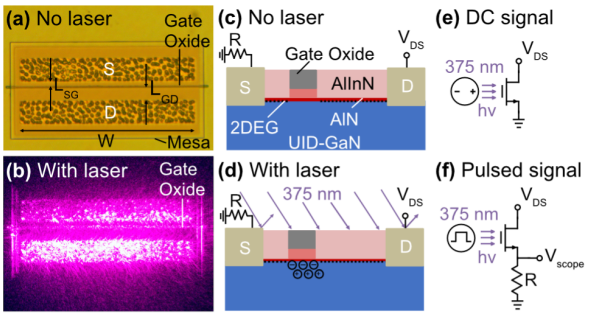

Fig. 1. Top-down microscope images of an LT-HEMT with and without laser illumination. (a) Shows the fabricated device with no laser light and labeled with dimensions. (b) Shows the device illuminated by a 375 nm laser, which is focused in the shape of an oval with an area of 1.64×10^{-4} cm^2. Cross-sectional schematics of the LT-HEMT (c) without laser light where the 2DEG under the gate oxide is depleted of carriers and (d) with laser light where carriers are generated to turn on the HEMT. Circuit diagram for the device under (e) DC and (f) pulsed conditions.

TABLE I
DIMENSIONS OF THE FABRICATED AND CHARACTERIZED LT-HEMTS AND CORRESPONDING 2DEG RESISTANCES PRESENTED IN THIS WORK

FET Type	Channel Width (μm)	L_G (μm)	L_{GS} (μm)	L_{GD} (μm)	L_{DS} (μm)	R_{2DEG} (Ω)
FETa	190	2	7	12	21	28.0
FETb	190	5	10	15	30	36.8
FETc	190	2	11.5	16.5	30	41.2

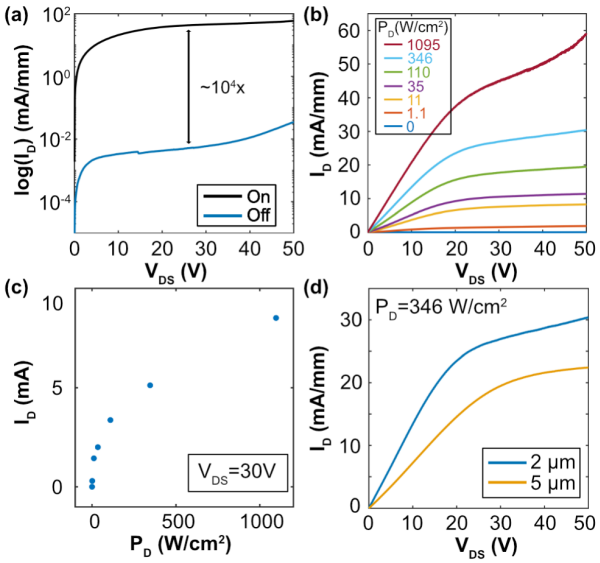

Fig. 2. (a) Plot of the log of the drain current (log(I_D)) versus drain-source voltage (V_{DS}) for an LT-HEMT without (off) and with maximum laser illumination (on). (b) Plot of I_D versus V_{DS} for varying laser power densities (P_D) ranging from 0 to 1095 W/cm^2 adjusted using neutral density filters. (c) Plot of drain current versus power density at $V_{DS} = 30$V. As the power density increases, the current gain saturates. (d) Plot of I_D versus V_{DS} for LT-HEMTs with 2 μm (FETa) and 5 μm (FETb) long oxidized gates at a laser power density (P_D) of 346 W/cm^2. As the area of the oxidized region decreases, the on-resistance decreases.

the LT-HEMTs, and the power is adjusted using neutral density filters. A microscope image of the LT-HEMT under illumination is shown in Fig. 1(b), displaying light scattering from the contacts, mesa edges, and gate oxide. Fig. 1(c) shows a cross-sectional schematic of the LT-HEMT with no laser light (off-state). The 2DEG underneath the oxidized regions is depleted, resulting in E-mode operation. Indium in the AlInN region underneath the oxide migrates to the surface during oxidation, causing compositional changes, as observed previously [29]. This changes the polarization fields and depletes the 2DEG. Fig. 1(d) shows a schematic of an illuminated device. The GaN absorbs the light throughout the area between the source and drain and the light generates carriers underneath the oxide within the depleted region. A conduction path is created between the 2DEGs, turning on the HEMT. Fig. 1(e) shows the circuit diagram under DC testing. Electrical characteristics are measured with a semiconductor parameter analyzer under different light powers on the gate.

Switched conditions are used to determine the LT-HEMT's maximum switching frequency and rise-fall times. The test circuit is shown in Fig. 1(f). A pulse generator is connected to the laser power supply to pulse the laser signal and vary power. The laser's power supply has a maximum modulation frequency of 100 kHz. A 68-ohm load resistor is connected in series with the LT-HEMT using coaxial cables. A 30 V bias is applied to the HEMT using the DC power supply. Finally, the oscilloscope is used to measure the switching performance of the LT-HEMT with a high-frequency voltage probe connected across the resistor and the change in current is observed on the oscilloscope. The laser's power and switching times are measured separately with a 1 GHz Si PIN detector connected directly to the oscilloscope.

While under bias and illumination, the resistance and switching speeds of the LT-HEMTs stabilize after ~30 minutes (burn-in). The burn-in increases resistance by ~2 times and decreases fall times from ~6 μs to <1 μs. The burn-in persists even after remeasuring days later. One explanation is that electrical current permanently affects the gate oxide and interface trap states by the successive switching. The burn-in is previously seen in AlInN/GaN HEMTs with oxidized gates [28]. All the devices were burned in before measuring and testing of several devices showed similar results.

III. RESULTS AND DISCUSSION

Fig. 2(a)-(c) demonstrates the on- and off-state currents, the output characteristics, and current gain for the 2 μm long gate (FETa). In Fig. 2(a), the drain current (log(I_D)) vs. drain-source voltage (V_{DS}) is plotted before and after illumination. The LT-HEMTs have an on/off ratio of ~10^4. Fig. 2(b) shows the I_D vs. V_{DS} characteristic with laser power densities from 0 to 1095 W/cm^2. The saturation current (I_{SAT}) increases with increasing laser power and peaks at ~60 mA/mm at 50 V. The LT-HEMTs can operate up to 100 V without breaking down. The laser energy is slightly below bandgap with a response of 6 orders of magnitude lower than 355 nm. The availability of shorter wavelength lasers will enable higher on/off ratios and I_{SAT}. We also observed light triggering with a 266 nm laser (harmonic generation of a 1046 nm diode laser), but it could not be easily switched. In Fig. 2(c), the current versus power density of the laser is plotted to visualize the current gain in the device. As the power density increases, the current gain in the devices saturates.

The on-state resistance (R_{on}) of the 2 μm (FETa) and 5 μm (FETb) long gates differs. Fig. 2(d) shows a plot of I_D versus

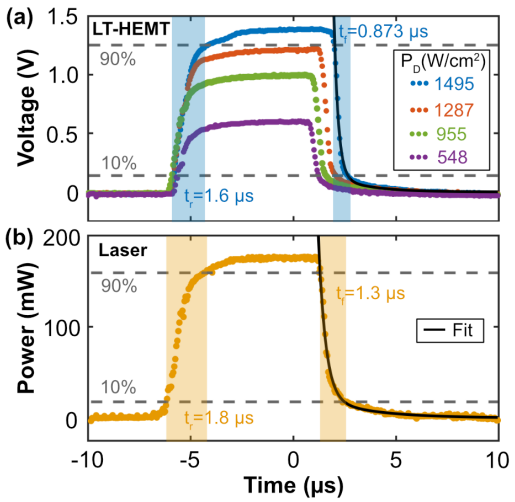

Fig. 3. Single-pulse response for the LT-HEMT and laser at 20 kHz with a 10 μs pulse width. (a) The response signal, measured across the resistor, for the LT-HEMT is plotted for different laser powers. The rise (t_r) and fall (t_f) times are shown for the LT-HEMT at the highest laser power and are denoted with a blue bar. (b) Laser rise and fall times as measured with a Si photodetector connected directly to the oscilloscope. For both the LT-HEMT and laser, a bi-exponential fit to the decay is displayed (black line), $y = A*\exp(-t/\tau_1)+B*\exp(-t/\tau_2)$ [31]. The LT-HEMT decay curve fits result in $\tau_1 = 0.21$ μs and $\tau_2 = 1.63$ μs.

V_{DS} at a laser power density of 346 W/cm^2 for both. The series resistances before saturation are 3.94 kΩ and 7.4 kΩ for the 2 μm and 5 μm gates, respectively. Changes in L_{DS} play a minor role in resistance since the resistivity under the oxide is over a hundred times larger than R_{2DEG} (Table I). Factoring out R_{2DEG}, the resistance under the gate is 1.9 times higher in the 5 μm long gate. All other dimensions are equal, so the difference in gate resistance should be the ratio of the gate lengths, or 2.5 times. The discrepancy suggests the gate dimensions affect how the 2DEG is depleted under the oxidized gate. One explanation for the difference is that the oxidation kinetics vary for the two stripe lengths. The 2-um-long gate has a small area exposed to the oxidant, leading to variations in oxidation depth and 2DEG depletion. Reducing the oxide length is an approach to further reducing the on-resistance.

Switching measurements are performed on 2 μm long oxidized devices (FETc). The rise (t_r) and fall (t_f) times of the LT-HEMTs are measured with the laser pulsed at 20 kHz with a 10 μs pulse width, at maximum power. Figs. 3(a) and (b) show the response for a single pulse for the LT-HEMT and laser. The t_r and t_f times are the switching times between 90% and 10% of the maximum signal. The LT-HEMT's t_r and t_f are 1.6 μs and 0.873 μs, respectively. The saturation in the on-current versus laser power under pulsing matches the trend observed in Fig. 2(c). The rise-fall times are considerably faster than other GaN-based PDs and PTs, with 100 μs or more switching times [12], [14], [16], [18], [19], [20], [21], [30], [31], [32], [33]. Table II compares current and switching capabilities for this work and other GaN-based PDs and PTs. The on/off current ratio can be improved by using a shorter wavelength laser to increase the on current or changing the oxidation time to alter the R_{on}.

The LT-HEMTs have a small amount of current (<1% of peak) that continues for ∼1 ms after turn-off, potentially the remnants of PPC. Two possible mechanisms counteract PPC:

TABLE II
COMPARISON OF GaN-BASED PHOTODIODES AND PHOTOTRANSISTORS

Structure	WL (nm)	Dark Current	I_{on}/I_{off}	Rise Time	Fall Time
GaN Schottky [12]	360	-	-	115 µs	120 µs
GaN PIN [33]	365	-	-	75 µs	110 µs
Recessed barrier AlGaN/GaN HEMT [30]	365	10 pA	$1x10^8$	32 ms	76 ms
Schottky gate AlGaN/GaN HEMT [16]	365	$4x10^{-6}$ (mA/mm)	$3.6x10^7$	40 ms	20 ms
p-GaN gate AlGaN/GaN HEMT [21]	365	$2.8x10^{-8}$ (mA/mm)	$1.7x10^8$	12.2 ms	8.9 ms
Enhanced p-GaN gate AlGaN/GaN HEMT [31]	345	$2.6x10^{-10}$ (mA/mm)	$1.42x10^{11}$	2 µs	128.4 µs
This work	375	$5.9x10^{-3}$ (mA/mm)	$7.6x10^3$	1.6 µs	0.873 µs

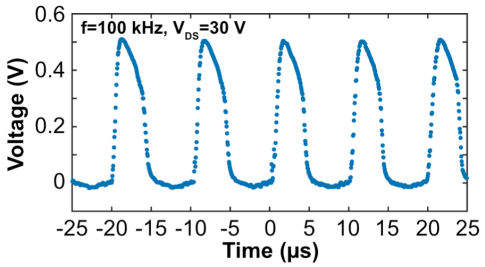

Fig. 4. Switching response of the LT-HEMT pulsed at maximum laser powers and at 100 kHz with 5 μs pulse widths and $V_{DS} = 30$V.

indium surface migration during oxidation, altering the AlInN composition, and vacancies acting as recombination centers in the AlInN underneath the oxide to reduce the decay time. Another hypothesis is epitaxial defects that cause PPC are reduced during high-temperature oxidation. This vacancy or defect modification in the semiconductor layers under the oxide aids in the switching times, since the laser light is below the bandgap. The exact mechanism requires further study.

Fig. 3(b) shows the laser's response at full power. The rise and fall times are measured as 1.8 μs and 1.3 μs, respectively. The faster LT-HEMT response is attributed to non-linear generation-recombination dynamics. The fall times should be related to minority carrier recombination rates in GaN but are slower than expected because the laser power supply limits the switching speed. When the laser power is decreased, both the LT-HEMT and laser fall times increase together.

Fig. 4 shows the switching response of an LT-HEMT with a 2 μm gate length (FETc). It is pulsed at 100 kHz with 5 μs pulse widths while biased at 30 V. The minimum pulse width is limited to 5 μs because of the switching limitations of the laser's power supply.

IV. Conclusion

Light-triggered AlInN/GaN HEMTs with low dark currents, 100 kHz frequency response, and fast switching speeds below 1 μs are achieved. The oxidized gates enable E-mode operation and fast switching speeds.

Acknowledgment

The authors want to acknowledge NTT-AT for growing the HEMT wafer used in this study.

REFERENCES

[1] J. Millán, P. Godignon, X. Perpiñà, A. Pérez-Tomás, and J. Rebollo, "A survey of wide bandgap power semiconductor devices," *IEEE Trans. Power Electron.*, vol. 29, no. 5, pp. 2155–2163, May 2014, doi: 10.1109/TPEL.2013.2268900.

[2] I. C. Kizilyalli, T. Prunty, and O. Aktas, "4-kV and 2.8-mΩ-cm^2 vertical GaN p-n diodes with low leakage currents," *IEEE Electron Device Lett.*, vol. 36, no. 10, pp. 1073–1075, Oct. 2015, doi: 10.1109/LED.2015.2474817.

[3] C. Mion, J. F. Muth, E. A. Preble, and D. Hanser, "Accurate dependence of gallium nitride thermal conductivity on dislocation density," *Appl. Phys. Lett.*, vol. 89, no. 9, Aug. 2006, Art. no. 092123, doi: 10.1063/1.2335972.

[4] S. K. Mazumder and T. Sarkar, "Optically activated gate control for power electronics," *IEEE Trans. Power Electron.*, vol. 26, no. 10, pp. 2863–2886, Oct. 2011, doi: 10.1109/TPEL.2009.2034856.

[5] S. K. Pandey, S. Rajput, V. Kaushik, R. D. Mishra, P. Babu, and M. Kumar, "Optically triggered AlGaN/GaN semiconductor power transistor with bi-layer anti-reflecting structure," *Proc. SPIE*, vol. 62, no. 12, Dec. 2023, Art. no. 127102, doi: 10.1117/1.oe.62.12.127102.

[6] S. L. Rumyantsev, M. E. Levinshtein, T. Saxena, M. S. Shur, L. Cheng, J. W. Palmour, and A. Agarwal, "Optical triggering of 4H-SiC thyristors (18 kV class) to high currents in purely inductive load circuit," *Semicond. Sci. Technol.*, vol. 29, no. 11, Nov. 2014, Art. no. 115003, doi: 10.1088/0268-1242/29/11/115003.

[7] J. S. Sullivan and J. R. Stanley, "Wide bandgap extrinsic photoconductive switches," *IEEE Trans. Plasma Sci.*, vol. 36, no. 5, pp. 2528–2532, Oct. 2008, doi: 10.1109/TPS.2008.2002147.

[8] J. Vobecký, H.-J. Schulze, P. Streit, F.-J. Niedernostheide, V. Botan, J. Przybilla, U. Kellner-Werdehausen, and M. Bellini, "Silicon thyristors for ultrahigh power (GW) applications," *IEEE Trans. Electron Devices*, vol. 64, no. 3, pp. 760–768, Mar. 2017, doi: 10.1109/TED.2016.2638476.

[9] X. Wang, H. Pu, Q. Liu, L. An, X. Tang, and Z. Chen, "Demonstration of 4H-SiC thyristor triggered by 100-mW/cm^2 UV light," *IEEE Electron Device Lett.*, vol. 41, no. 6, pp. 824–827, Jun. 2020, doi: 10.1109/LED.2020.2988913.

[10] L. Hu, J. Huang, X. Yang, X. Shen, and Y. Sun, "Analysis of the avalanche operation of a GaN photoconductive semiconductor switch," *IEEE Trans. Electron Devices*, vol. 70, no. 11, pp. 5778–5785, Nov. 2023, doi: 10.1109/TED.2023.3313572.

[11] Y. Chen, H. Lu, D. Chen, F. Ren, R. Zhang, and Y. Zheng, "High-voltage photoconductive semiconductor switches fabricated on semi-insulating HVPE GaN:Fe template," *Phys. Status Solidi C*, vol. 13, nos. 5–6, pp. 374–377, May 2016, doi: 10.1002/pssc.201510210.

[12] W. Mou, L. Zhao, L. Chen, D. Yan, H. Ma, G. Yang, and X. Gu, "GaN-based Schottky barrier ultraviolet photodetectors with graded doping on patterned sapphire substrates," *Solid-State Electron.*, vol. 133, pp. 78–82, Jul. 2017, doi: 10.1016/j.sse.2017.04.008.

[13] X. Zou, X. Zhang, Y. Zhang, Q. Lyu, C. W. Tang, and K. M. Lau, "GaN single nanowire p–i–n diode for high-temperature operations," *ACS Appl. Electron. Mater.*, vol. 2, no. 3, pp. 719–724, Mar. 2020, doi: 10.1021/acsaelm.9b00801.

[14] M. A. Khan, Q. Chen, J. N. Kuznia, C. J. Sun, and M. S. Shur, "Gated photodetector based on GaN/AlGaN heterostructure field effect transistor," *Electron. Lett.*, vol. 31, no. 5, pp. 398–400, Mar. 1995.

[15] S.-H. Baek, G.-W. Lee, C.-Y. Cho, and S.-N. Lee, "Gate-controlled amplifiable ultraviolet AlGaN/GaN high-electron-mobility phototransistor," *Sci. Rep.*, vol. 11, no. 1, p. 7172, Mar. 2021, doi: 10.1038/s41598-021-86575-7.

[16] H. Zhang, F. Liang, K. Song, C. Xing, D. Wang, H. Yu, C. Huang, Y. Sun, L. Yang, X. Zhao, H. Sun, and S. Long, "Demonstration of AlGaN/GaN-based ultraviolet phototransistor with a record high responsivity over 3.6 $\times$ 10^7 A/W," *Appl. Phys. Lett.*, vol. 118, no. 24, Jun. 2021, Art. no. 242105, doi: 10.1063/5.0055468.

[17] A. Mojab, Z. Hemmat, H. Riazmontazer, and A. Rahnamaee, "Introducing optical cascode GaN HEMT," *IEEE Trans. Electron Devices*, vol. 64, no. 3, pp. 796–804, Mar. 2017, doi: 10.1109/TED.2017.2657498.

[18] M. Martens, J. Schlegel, P. Vogt, F. Brunner, R. Lossy, J. Würfl, M. Weyers, and M. Kneissl, "High gain ultraviolet photodetectors based on AlGaN/GaN heterostructures for optical switching," *Appl. Phys. Lett.*, vol. 98, no. 21, May 2011, Art. no. 211114, doi: 10.1063/1.3595303.

[19] S. Kumar, A. S. Pratiyush, S. B. Dolmanan, S. Tripathy, R. Muralidharan, and D. N. Nath, "UV detector based on InAlN/GaN-on-Si HEMT stack with photo-to-dark current ratio > 10^7," *Appl. Phys. Lett.*, vol. 111, no. 25, Dec. 2017, Art. no. 251103, doi: 10.1063/1.5004024.

[20] M. Iwaya, S. Miura, T. Fujii, S. Kamiyama, H. Amano, and I. Akasaki, "High-performance UV detector based on AlGaN/GaN junction heterostructure-field-effect transistor with a p-GaN gate," *Phys. Status Solidi C*, vol. 6, no. S2, pp. S972–S975, Jun. 2009, doi: 10.1002/pssc.200880815.

[21] Q. Lyu, H. Jiang, and K. M. Lau, "High gain and high ultraviolet/visible rejection ratio photodetectors using p-GaN/AlGaN/GaN heterostructures grown on Si," *Appl. Phys. Lett.*, vol. 117, no. 7, Aug. 2020, Art. no. 071101, doi: 10.1063/5.0011685.

[22] M. Hou, H. So, A. J. Suria, A. S. Yalamarthy, and D. G. Senesky, "Suppression of persistent photoconductivity in AlGaN/GaN ultraviolet photodetectors using in situ heating," *IEEE Electron Device Lett.*, vol. 38, no. 1, pp. 56–59, Jan. 2017, doi: 10.1109/LED.2016.2626388.

[23] H. M. Chen, Y. F. Chen, M. C. Lee, and M. S. Feng, "Persistent photoconductivity in n-type GaN," *J. Appl. Phys.*, vol. 82, no. 2, pp. 899–901, Jul. 1997, doi: 10.1063/1.365859.

[24] J. Z. Li, J. Y. Lin, H. X. Jiang, M. Asif Khan, and Q. Chen, "Persistent photoconductivity in a two-dimensional electron gas system formed by an AlGaN/GaN heterostructure," *J. Appl. Phys.*, vol. 82, no. 3, pp. 1227–1230, Aug. 1997, doi: 10.1063/1.365893.

[25] C. H. Qiu and J. I. Pankove, "Deep levels and persistent photoconductivity in GaN thin films," *Appl. Phys. Lett.*, vol. 70, no. 15, pp. 1983–1985, Apr. 1997, doi: 10.1063/1.118799.

[26] M. R. Peart, X. Wei, D. Borovac, W. Sun, N. Tansu, and J. J. Wierer, "Thermal oxidation of AlInN for III-nitride electronic and optoelectronic devices," *ACS Appl. Electron. Mater.*, vol. 1, no. 8, pp. 1367–1371, Aug. 2019, doi: 10.1021/acsaelm.9b00266.

[27] E. Palmese, M. R. Peart, D. Borovac, R. Song, N. Tansu, and J. J. Wierer, "Thermal oxidation rates and resulting optical constants of $Al_{0.83}In_{0.17}N$ films grown on GaN," *J. Appl. Phys.*, vol. 129, no. 12, Mar. 2021, Art. no. 125105, doi: 10.1063/5.0035711.

[28] E. Palmese, H. Xue, S. Pavlidis, and J. J. Wierer, "Enhancement-mode AlInN/GaN high-electron-mobility transistors enabled by thermally oxidized gates," *IEEE Trans. Electron Devices*, vol. 71, no. 2, pp. 1003–1009, Feb. 2024, doi: 10.1109/TED.2023.3343313.

[29] E. Palmese, H. Xue, R. Song, and J. J. Wierer, "Thermal oxidation of lattice mismatched $Al_{1-x}In_xN$ films on GaN," *e-Prime, Adv. Electr. Eng., Electron. Energy*, vol. 5, Sep. 2023, Art. no. 100208, doi: 10.1016/j.prime.2023.100208.

[30] P. F. Satterthwaite, A. S. Yalamarthy, N. A. Scandrette, A. K. M. Newaz, and D. G. Senesky, "High responsivity, low dark current ultraviolet photodetectors based on two-dimensional electron gas interdigitated transducers," *ACS Photon.*, vol. 5, no. 11, pp. 4277–4282, Nov. 2018, doi: 10.1021/acsphotonics.8b01169.

[31] H. Wang, H. You, Y. Xu, X. Sun, Y. Wang, D. Pan, J. Ye, B. Liu, D. Chen, H. Lu, R. Zhang, and Y. Zheng, "High-responsivity and fast-response ultraviolet phototransistors based on enhanced p-GaN/AlGaN/GaN HEMTs," *ACS Photon.*, vol. 9, no. 6, pp. 2040–2045, Jun. 2022, doi: 10.1021/acsphotonics.2c00177.

[32] Y. Wang, C. Liu, H. Qian, H. Liu, L. Han, X. Wang, W. Gao, and J. Li, "Light-triggered 2D electron gas in a GaN-based HEMT with sandwiched p-GaN layers," *Opt. Lett.*, vol. 48, no. 16, pp. 4376–4379, Aug. 2023, doi: 10.1364/ol.499084.

[33] W. Xu, Y. Shi, F. Ren, D. Zhou, L. Su, Q. Liu, L. Cheng, J. Ye, D. Chen, R. Zhang, Y. Zheng, and H. Lu, "Magnesium ion-implantation-based gallium nitride p-i-n photodiode for visible-blind ultraviolet detection," *Photon. Res.*, vol. 7, no. 8, p. 48, 2019, doi: 10.1364/prj.7.000b48.